Check for updates

New details of assembling bioactive films from dispersions of amphiphilic molecules on titania surfaces†

Leonardo Francisco Gonçalves Dias, [ab] Stephani Stamboroski, [af] Michael Noeske,*[a] Dirk Salz,[a] Klaus Rischka, [a] Renata Pereira,[ah] Maria do Carmo Mainardi, [ag] Marina Honorato Cardoso,[c] Martin Wiesing,[a] Erika Soares Bronze-Uhle,[d] Rodrigo Barros Esteves Lins[e] and Paulo Noronha Lisboa-Filho[b]

Tailoring the surface properties of materials for biomedical applications is important to avoid clinical complications. Forming thin layers of amphiphilic molecules with apolar regions that facilitate attractive intermolecular interactions, can be a suitable and versatile approach to achieve hydrophobic surface modification and provide functional antibacterial properties. Aiming to correlate layer structure and properties starting from film formation, octadecylphosphonic acid (**ODPA**) and dimethyloctadecyl (3-trimethoxysilylpropyl) ammonium chloride (**DMOAP**) layers were adsorbed onto smooth titania surfaces. Then the films were studied by atomic force microscopy (AFM) and X-ray Photoelectron Spectroscopy (XPS), and their interactions with aqueous environments were characterized by contact angle and zeta potential measurements. In addition, antibacterial assays were performed using *E. coli* and *S. mutants* to reveal the antibacterial properties effected by the surface modification. Immediately after sputter deposition, titania was hydrophilic; however, after air storage and adsorption of **DMOAP** or **ODPA**, an increase in the water contact angle was observed. XPS investigations after layer formation and after antibacterial tests revealed that the attachment of layers assembled from **ODPA** on titania substrates is considerably stronger and more stable than that observed for **DMOAP** films. Heat treatment strongly affects **DMOAP** layers. Furthermore, **DMOAP** layers are not stable under biological conditions.

Introduction

The design of novel functional biomaterials depends on tailoring their multiscale structures.[1,2] Surface modification is a suitable strategy to enhance the properties of biomaterials such as biocompatibility and antibacterial efficacy.[3] Different

[a]*Fraunhofer Institute for Manufacturing Technology and Advanced Materials IFAM, Bremen, Germany. E-mail: michael.noeske@ifam.fraunhofer.de*

[b]*São Paulo State University – UNESP, School of Science, Department of Physics, Brazil*

[c]*Department of Biochemistry, Bauru School of Dentistry, Sao Paulo University – USP, Bauru, SP, Brazil*

[d]*Department of Operative Dentistry, Endodontics and Dental Materials, Bauru School of Dentistry, Sao Paulo University – USP, Bauru, SP, Brazil*

[e]*Paraiba State University – João Pessoa, PB, Brazil*

[f]*Institute for Biophysics, University of Bremen, Otto-Hahn-Allee 1, 28359 Bremen, Germany*

[g]*School of Dentistry, Herminio Ometto University Center, Araras, SP, Brazil*

[h]*Department of Restorative Dentistry, Operative Dentistry Division, Piracicaba Dental School, University of Campinas (UNICAMP), Avenida Limeira 901, Zip code 13414-903, Piracicaba, SP, Brazil*

† Electronic supplementary information (ESI) available. See DOI: 10.1039/d0ra06511k

procedures are well established, such as depositing silver as an antibacterial component or immobilizing functional molecules on medical products.[4,5] Aiming to introduce antibacterial properties to medical devices, a valid alternative is grafting chemically reactive quaternary ammonium compounds (QACs), such as dimethyloctadecyl (3-trimethoxysilylpropyl) ammonium chloride (**DMOAP**). **DMOAP** has a quaternary ammonium group that is separated by a propylene spacer from a hydrophilic tri-methoxy silane group and bound to an aliphatic octadecyl chain ($C_{26}H_{58}NO_3SiCl$), which is responsible for its hydrophobicity.[6] **ODPA** (octadecylphosphonic acid) also contains a hydrophobic chain, and its hydrophilicity is due to a protonated or deprotonated phosphonate group. The immobilization of ODPA can also form antibacterial response on surfaces.[7] Structural formulas of linear **DMOAP** and **ODPA** conformations are presented in Fig. 1. Hydrophobic surfaces can be suitable for biomedical devices to avoid protein adsorption, increase the surface charge in contact with aqueous fluids, and establish an antimicrobial effect.[7–10] Modifications of surface charge play an important role in achieving antimicrobial efficacy in different bacteria-containing media.[11] Although a long alkyl chain could increase the surface hydrophobicity and influence bacteria

(a) Dimethyloctadecyl[3-(trimethoxysilyl)propyl]ammonium chloride
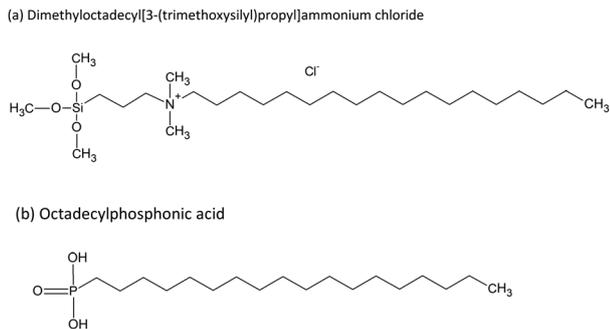
(b) Octadecylphosphonic acid

Fig. 1 Linear structure of (a) DMOAP and (b) ODPA.

adsorption, the presence of a cation induces electrostatic interaction with the bacteria phospholipid bilayer.[12]

As reviewed by Elena and Miri,[13] QACs can be immobilized on different surfaces, from cotton fibers to metal oxides, apart from being incorporated in the synthesis of resins for dental applications.[14] Quaternary ammonium compounds present antibacterial activity even when their head groups are hydrolysed in a solution; however, non-immobilized QACs are often active surface water contaminants and can potentially cause environment damage.[15] Thereby, immobilization of QACs on a surface while largely maintaining their activity is a desirable but challenging procedure, which aims to provide a non-release system and avoid environment impact.[16,17] For instance, Meng et al. demonstrated that when immobilized on cellular membranes, DMOAP can maintain its antibacterial efficacy in various conditions, such as pH of 3.5 and temperature of 50 °C.[6]

Despite its attested antibacterial efficacy, the mechanism of action of DMOAP has not been fully elucidated. The mechanism has been described in the following manner: attraction between the positively charged DMOAP layer and the negatively charged bacteria cell membrane occurs supported by van der Waals interactions between the respective DMOAP or phospholipid hydrophobic tails.[18] The electrostatic attraction leads to an ionic interaction causing the transport of divalent cations (Ca^{2+} and Mg^{2+}), inducing membrane disruption and consequent death of the bacteria.[18,19] The surface charge density induced by the ammonium cation plays a crucial role in the antibacterial activity. Asri et al., using AFM measurements, reported that immobilized QAC has a strong interaction with Staphylococcus epidermidis, and the force of interaction with the bacteria surface was five to six times greater than usually found for bacteria adhesion on surfaces, which are in a range of 1 nN.[18] He et al. observed that when E. coli attaches on a DMOAP surface, a distortion of the cell membrane leads to its rupture.[20]

On the other hand, immobilized ODPA provides antibacterial properties due to the increased surface hydrophobicity, consequently avoiding the adsorption of some bacteria.[7] Zhang et al. reported that ODPA immobilization on titania nanotubes not only avoids bacterial adherence but can also modulate the release of Sr and Zn when these are dopants of the nanotubes.[7] ODPA is irreversibly adsorbed on $Ti_{0.5}Al_{0.5}N$ surfaces forming a non-release system, as reported by Theile-Rasche et al.[21]

In addition to characterization, useful tools for revealing the arrangement of DMOAP and ODPA layers on surfaces are contact angle measurements, atomic force microscopy, and X-ray photoelectron spectroscopy. DMOAP and ODPA modify the wettability of the surface due to their long alkyl chains. Besides the binding situation and area density of the functional groups of those molecules, quaternary ammonium for DMOAP and phosphonate for ODPA can be detected by XPS.[18,20–22]

For tailoring the physicochemical properties in aqueous environment, such as zeta potential and wettability of the layer systems formed by immobilized DMOAP and ODPA, details about the adsorption process are important to understand. To elucidate the effects of process parameters in forming bioactive layers, combining microscopic and spectroscopic studies with nanoscale sensitivity and a layer build-up on flat and chemically well-defined substrates is innovative, as was shown for designing highly active antifouling layers[23] and antimicrobial films, promoting protein adsorption,[24] and verifying the influence of electrolytes on contact angle.[25]

For achieving antibacterial contact-activity, numerous approaches for tailoring substrate surface properties have been reported. Surface structure, wettability, composition, and time-dependent release properties in aqueous environment have been generally assessed. These studies revealed that increased antimicrobial activity is promoted by adjusting the surface roughness instead of providing smooth substrate surfaces; introducing amphiphilic moieties in films that will be in contact with phospholipid-based bacterial membranes; integrating molecular groups that affect the surface charge like QACs; or facilitating the release of metal ions from bulk film regions that are not exposed to the convective transport for permitting longer-term activity of antimicrobial coatings (AMC). The underlying antimicrobial strategies may comprise several components. Among them, providing anti-adhesive surfaces to avoid or retard microbial attachment,[26] contact-active surfaces that are based on immobilized and not released active species,[3,27] and biocide-releasing surfaces.[28]

Tailoring strongly attaching films composed of amphiphilic molecules with respect to their antibacterial activity has been reported based on approaches considering thick films[29,30] and polymeric[20] or hybrid[18] bulk materials containing quaternary ammonium species. For such substrates, a substantial conformational freedom of the molecular entities exposing the quaternary ammonium species may be expected in a swollen state in the presence of aqueous environments containing bacteria.[20]

In addition to chemical modifications, the topography of a surface can significantly affect its hygienic status, either beneficially (reducing microbial retention) or negatively (increasing retention).[28] Findings of surface charge densities around 1.5×10^{15} cm^{-2} or even 10^{16} cm^{-2} for monovalent ammonium cations are based on calculations considering the geometric surface area of rough substrates rather than on their active surface area, since monolayer densities do not exceed 5×10^{14} atoms cm^{-2}, even of unbranched nonanethiols on gold.[31,32]

The present study aims to achieve a more profound understanding about material-related properties governing a contact-

killing ability from the interaction between bacteria and substrates containing quaternary ammonium species by assessing dynamic effects in the bacteria/QAC interface. Properties of silane-based layers and their mechanism of immobilization need to be explored to devise deposition processes and exploit their versatility for surface modification.[33] In addition, systematic studies for governing the contact formation and its effect by tailoring the substrate surface were performed. A versatile and well-controlled multi-step approach was developed for designing the AMC surface. Starting from a topologically well-defined substrate that may be smooth or microstructured, thin biocompatible and non-cytotoxic titania nanofilms were deposited as a base for the application of AMCs.

As immobilizing QACs in thin layers may strongly restrict conformational freedom of the molecules, **DMOAP** films with different thickness were studied starting from the monolayer regime to demonstrate the versatility of our approach. Studies relating layer structure and its biological activity are scarce and need to be clarified;[34] thus, this work explores this gap in the literature, showing well characterized layers before and after biological assays. Smooth substrates were used to restrict the potential bacteria/QAC interface to the geometrical surface area. Inorganic oxidic titania substrate material was also used to exclude swelling effects upon exposure to aqueous environments. Finally, **ODPA** SAMs were used, which like **DMOAP** contain hydrophobic octadecyl molecular tails. The orientation of amphiphilic molecules in such well-ordered monolayers provides a reference for working out the effects of molecular orientation observed in thin **DMOAP** films.

Materials and methods

Materials

Silicon wafers (diameter of 100 mm) from Si-Mat and glass slides (75 × 25 mm) from Thermo Scientific® were used as substrates. Titanium dioxide was obtained from a metallic titanium target that was used for sputter-deposition in an oxygen containing atmosphere. A methanol-based mixture of 42 wt% dimethyloctadecyl(3-(trimethoxysilyl)propyl)ammonium chloride (**DMOAP**) (CAS 27668-52-6) and 8 wt% of (3-chloropropyl)trimethoxysilane from SIGMA-ALDRICH® and octadecylphosphonic acid (**ODPA**) (CAS 4724-47-4) from TCI® Germany were employed for the layer formation experiments on sputter-deposited TiO_2 on silicon wafers and glass. Ethanol 99% (CAS 64-17-5) from Labochem® was used as solvent to prepare **DMOAP** and **ODPA** solutions.

Preparation of bulk DMOAP and ODPA for XPS investigation

To prepare samples for XPS investigations and bioactivity tests, **DMOAP** was dropped as received in a silicon wafer, and after evaporation of the solvent the obtained specimen was henceforth called "bulk **DMOAP**" sample. A second sample was prepared by exposing the obtained solid deposit product to water at room temperature for distinct periods and subsequently dried. The thus prepared samples were called "water exposed **DMOAP**". As a reference for the biological assay,

DMOAP was dropped on titania surface and the solvent was left to dry in air. The procedure was repeated twice. The final sample named "Blot **DMOAP**" was a thick layer heated overnight at 100 °C in an oven at ambient atmosphere.

For preparing the so-called "bulk ODPA" samples, a small quantity of the **ODPA** product powder was dissolved in 99% ethanol to obtain a turbid suspension. A drop was placed on a silicon wafer and gently blown dry using an air stream generated by a hand bellow to remove the solvent excess.

Surface preparation – film deposition

A silicon wafer was cut in two different sizes, 3 × 5 mm and 20 × 20 mm, and the respective pieces were used for XPS measurements and biological assays, respectively. After the cutting procedure, the substrates were ultrasonically cleaned in water for 10 minutes. Glass slides were used as received. Subsequently, the substrates were placed in a vacuum chamber then pumped until reaching a pressure of 10^{-5} hPa. The argon flux was adjusted to 120 sccm. Finally, the titanium dioxide deposition started.

First in the deposition process, the target was sputtered without the presence of oxygen for 30 s. Afterwards, oxygen was slowly added into the chamber, using a flux of 9 sccm, for 900 s. A power of 2300 W and maximum bias of 765 V were applied. For all adsorbents, the layer formation experiments were performed five minutes after sample removal from the chamber.

Solution preparation

Two different solutions containing **DMOAP** were prepared, similar as described by Torkelson et al.[35] A volume of 0.6 mL of 42 wt% **DMOAP** solution in methanol was diluted in 49.4 mL of 99% ethanol to produce the first working solution. For the second solution, the same procedure was followed and 10 drops (approx. 50 μL) of 1 M aqueous hydrochloric acid (previously prepared) were added after mixing the alcoholic liquids. The solutions were called "**DMOAP**-N" (without acid addition) and "**DMOAP**-A" (with acid addition).

ODPA solution was prepared as follows: 167.25 mg of **ODPA** were dissolved in 50 mL of 99% ethanol, establishing a concentration of 1 mM.

All immersion experiments of titania-coated substrates were performed approximately 30 minutes after solution preparation. In this freshly prepared state, the solutions visually appeared transparent, clear, and colourless and remained as such during the immersion procedures.

Layer formation on TiO_2

The procedures described below were used for all titania-coated substrates. All samples were gently rinsed (either in distilled water or ethanol) after immersion in **DMOAP** and **ODPA** solutions, and identified as "water rinsed" or "ethanol rinsed", respectively.

DMOAP adsorption

To attach **DMOAP** on the titanium dioxide surfaces, the substrates were immersed for 10 minutes or 24 hours at room temperature for each **DMOAP** solution. After the submersion time, the samples were removed from the solution and gently rinsed using distilled water from a wash bottle.

Two distinct drying procedures were employed. One method consisted in blowing the sample surface using clean compressed air after the washing procedure. For the second method, the samples were subsequently placed in an oven and completed drying in air at 100 °C overnight. To clarify the achieved samples, the descriptions of the preparation label and conditions are summarized in Table 1.

ODPA adsorption

ODPA was adsorbed also through sample immersion in **ODPA** solution for 18 hours. Additionally, the samples were removed and either of the two above-described washing procedures was followed. All samples were blown dry using air from a hand bellow to remove the excess solvent.

Atomic force microscopy

Nanomechanical surface properties were assessed applying a Bruker Dimension Icon3 with a Nanoscope V SPM control unit and the software NanoScope V9.40R1. The cantilever and tip used were selected according to the surface properties (XSC11-Pt, MikroMesh, force constant 40 nN nm^{-1}, tip radius < 20 nm). The calibration of the force constant was done by analyzing the thermal noise in combination with the Sader method.[36] The sensitivity was calibrated with the help of an Al_2O_3 substrate. The tip radius was determined using the image of a nano rough Ti reference sample. The quantification was carried out according to a modified Villarubia method that was implemented in NanoScope.[37] The QNM mode was used to quantify the nano-mechanical properties. For this purpose, the cantilever was excited non-resonantly at 2 kHz with amplitude of approximately 15 nm and indented into the surface with a depth up to a maximum of 2 nm; therefore, the indentation depth was approximately 10 nm.

Height profiles were obtained using a Nanosurf easyscan AFM device. The images were taken in a resolution of 512 × 512 pixels in different sizes. For this, the non-contact mode (variable force) was used with a scan line ratio of 2 seconds for each image and a cantilever with a force constant of 40 nN nm^{-1}. The post treatment was performed using the Gwyddion 2.55 software. First, a step line correction was applied. Then, the rows were aligned using a polynomial degree equal to five, and finally the strokes were corrected. The tip was a Tap190Al-G from Budget Sensors with a resonant frequency equals to 190 kHz.

Contact angle measurements

Contact angle measurements were performed immediately after the drying procedures. The analysed samples were TiO_2 sputter-deposited on glass slides. The measurements were evaluated using the mobile surface analyser – MSA from KRÜSS – at room temperature.

HPLC quality water and diiodomethane were used as probe liquids, and 2 μL of each liquid were simultaneously and automatically dropped on the surface. Then, the contact angle for each drop was recorded using the tangent method. Two distinct regions of the sample were analysed, and the mean contact angle for each liquid was calculated.

Changes of apparent water contact angles as a consequence of exposing **DMOAP** coated titania specimens to aqueous bacteria medium were recorded using a goniometer based (OCA15 Plus, Data Physics Instruments, Germany) approach and applying the sessile drop technique. For each measurement, 5 μL drops were formed using HPLC-grade water (Acros Organics, Germany) and the subsequent contact angles were taken and analysed by the software SCA202 (Data Physics Instruments, Germany). The reported contact angles are an average of at least three measurements for each sample.

XPS characterization

XPS characterization was carried out using a Kratos AXIS Ultra system with a monochromatized Al Kα X-ray source (energy $hv = $ 1486.6 eV). The base pressure of the analysis chamber was approximately 6×10^{-8} Pa. Spectra were acquired in the constant analyser energy mode using pass energies of 160 eV and an energy step of 0.444 eV for survey spectra and 20 eV and energy step of 0.066 eV for detail scans. Spectra fitting was performed using CasaXPS (v2.3.18, Casa Software Ltd). First, the binding energy scale of the spectra was aligned using the C1s

Table 1 Parameters of immersion, drying method, and sample name for **DMOAP**/titania films prepared from two different **DMOAP** solutions: **DMOAP**-N (without acid addition) and **DMOAP**-A (with acid addition)

Solution	Immersion time	Drying method	Sample name
DMOAP-N	10 minutes	Blown using compressed air	TiO_2/**DMOAP**-N 10 min
		Heated in an oven at 100 °C in air overnight	TiO_2/**DMOAP**-N 10 min heated
	24 hours	Blown using compressed air	TiO_2/**DMOAP**-N 24 h
		Heated in an oven at 100 °C in air overnight	TiO_2/**DMOAP**-N 24 h heated
DMOAP-A	10 minutes	Blown using compressed air	TiO_2/**DMOAP**-A 10 min
		Heated in an oven at 100 °C in air overnight	TiO_2/**DMOAP**-A 10 min heated
	24 hours	Blown using compressed air	TiO_2/**DMOAP**-A 24 h
		Heated in an oven at 100 °C in air overnight	TiO_2/**DMOAP**-A 24 h heated

signal at 285.0 eV of the aliphatic hydrocarbon species. Then, the signal area to analyse was set using a Shirley-type or linear background. Peak components were adjusted using the line shape GL(30). The full widths at half maximum (FWHM) for the C1s components were set to be equal. The created areas were fitted using the Marquardt–Levenberg algorithm. Based on the signal attenuation, the thickness of the adsorbed layers was estimated using the equation $d = \ln(y) \times \lambda$, where d is the thickness of the adsorbed layer, y is the ratio between the area of the Ti2p peak from the coated sample and the pristine sample, and λ is the inelastic mean free path of the electrons in the organic film (2.8 nm for Ti2p). For such estimation, the surface coating was assumed to be homogeneous.[1] A thickness of 0.6 nm was considered for the adventitious carbon layer on the titanium substrates.[38] An estimated layer thickness of an adsorbate was calculated based on the assumption that the adventitious carbon layer was replaced by the adsorbate layer. Atomic surface concentration values were calculated based on the simplifying geometric model assumption that the sample surface is homogeneously composed.

Zeta potential measurements

Zeta potential measurements were performed with different titanium dioxide samples deposited on glass slides.

The values were recorded using the SurPASS™ 3 device from Anton Paar at room temperature. The adjustable gap cell was used, and the gap adjusted to 100 μm. The pH was adjusted using 0.05 M solution of potassium hydroxide and 1 M solution of hydrochloric acid, respectively. The pH step was set to 0.75 in range from pH 8 to pH 4 (in this order) and measured with a pH meter sensor innate to the equipment. Before the measurements, the samples were stored for 24 hours in 2 hPa at room temperature. The error bars were estimated based on three distinct measurements according to the prepared samples.

Antibacterial assays

Escherichia coli bacterium (strain DSM 10290) was cultured in LB broth medium at 37 °C in aerobic conditions for 24 h. The growth culture suspension was centrifuged twice at 13 000 rpm for 5 minutes and suspended in PBS buffer. The optical density (OD) was measured at 600 nm in UV-Vis Specord 200 Analytic Jena spectrophotometer and the concentration was adjusted to 1×10^7 CFU mL^{-1} (with 0.06 OD corresponding to 2×10^8 CFU mL^{-1}) in minimal medium (1 : 100 of LB broth medium in PBS buffer). In a UV2 Sterilizing PCR Workstation, at room temperature, the samples ($n = 3$) were placed in sterile Petri dishes and received sprays of isopropanol 70%. The Petri dishes lids were opened, the working bench was closed, and the UV light was turned on for 30 minutes to sterilize the samples. Afterwards, 50 μL of bacterial solution were applied over each sample surface and a sterilized cover glass slip (18 × 18 mm) was placed to spread the drop over the substrate, according to the ISO 22196. Moreover, 2 mL of PBS was pipetted in the outlines of the Petri dishes to prevent evaporation. After incubation for 4 h at 37 °C, the cover glass slips were removed, and samples were carefully washed twice with distilled water to remove non-adherent or weakly adherent bacteria. The rinsed water was kept in a 2 mL centrifuge tube for further analysis. The samples were placed into a 50 mL centrifuge tube, which was filled with 15 mL of PBS buffer. The tubes were sonicated (Ultrasonic bath Sonorex RK100 Bandelin Electronic, Berlin, Germany) for three minutes and vortexed (Minishaker MS2, IKA – Werke GmbH & Co. KG, Staufen, Germany) for one minute to allow detachment of the adherent bacteria. The 24 h kinetic of both the non-adherent bacteria (from the rinsed water) and the bacteria detached from the sample were evaluated using Mithras LB 940 Microplate Reader (Berthold Technologies Ltd). Accordingly, 150 μL of each bacterial solution + 50 μL LB broth medium were pipetted in a well of a 96-well cell culture plate, which was placed in the device with all parameters set in the same conditions of the bacterium culture. The bacterial growth was related to the bacteria adhered on the surface of the samples, which after ultrasound and vortex remained alive and healthy to continue growing in suitable nutrients and temperature conditions. The bacterial growth from the rinsed water indicated a bacteriostatic effect of the sample, which inhibits the initial bacteria adhesion and further biofilm formation.

Testing with Gram-negative *E. coli* was introduced to the experimental design because **DMOAP** immobilized on polymers exhibited comparatively low minimum inhibitory concentrations (MIC) against *E. coli* and Gram-positive *S. aureus* as compared to *C. albicans fungus*.[39] Gram-negative *S. mutans* was chosen to be part of the conceptual design including bulk **DMOAP** specimens because of its relevance for dental research and considering the paramount objective was to identify if **DMOAP** shows an antibacterial effect against *S. mutans*.

Results and discussion

From the XPS spectroscopic point of view, the approach presented in this study profits from opting for smooth titania films. Moreover, on smooth substrates, the morphology of organic adsorbates can be accessed.[1] In comparison to silica or alumina adsorbents exhibiting contributions to the O1s signal at binding energies around 533.0 eV,[40,41] the O1s signal contributions related to oxide, hydroxide, or carbonate-related bulk and surface species, in case of titania substrates, are characterized by binding energies around 530.2 and 531.6 eV (± 0.1 eV), respectively.[40] This facilitates the spectroscopic characterization of the chemical environment of oxygen species in thin adsorbates of complex oxygen-containing amphiphilic adsorbates (like **ODPA** or **DMOAP**) on titania substrates.

XPS characterization

Bulk samples. Pure bulk material **ODPA** is composed of octadecylphosphonic acid molecules with a molecular structure displayed in Fig. 1; the molecule presents the following stoichiometry: $C_{18}H_{39}O_3P$. If a sample of this pure bulk material has a homogeneous composition, the atomic concentrations listed in Table 2 are expected based on this stoichiometry. Additionally, the measured atomic concentration (given in at%) of carbon is slightly higher than that displayed. The values

Table 2 Comparison between expected for homogeneous solid **ODPA** and obtained values from the XPS-based evaluations of atomic concentration

Atomic concentration (at%)	[C]			[O]			[P]	[Si]		
	Total	[C*–C/C*–H]	[C*–P]	Total	[P–O*H]	[P=O*]	Total	Total	[Bulk Si]	[SiO$_2^*$]
Expected value	81.92	77.33	4.59	13.64	9.09	4.54	4.54	0	—	—
Obtained from data evaluation	82.68	78.45	4.23	11.75	7.84	3.90	4.22	1.34	1.18	0.16

obtained for carbon, oxygen, and phosphorous are close to the stoichiometrically expected values. The concentration ratios [C]/[O], [C]/[P], and [O]/[P] indicate that a minor excess of carbon species is found at the sample surface, as shown in Table 3.

High resolution XPS spectra for the investigated bulk **ODPA** sample are presented in Fig. 2. C1s high resolution spectra were fitted using two contributions: one contribution at 285.0 eV from aliphatic carbon and the second centred at 285.8 eV due to C*–P species. From the molecular structure, the intensity for XPS signals related to C*–P and P*–C species in **ODPA** is expected to be equal to the atomic concentration [P] of phosphorus species in **ODPA** (4.5 at%). Based on an appropriate calibration of the applied relative RSF (relative sensitivity factors) for C1s and P2p in the XPS measurement, an area constraint was set to guarantee that the evaluated [C*–P] atomic concentration was equal to the evaluated atomic concentration [P] of phosphorus species in the investigated **ODPA** bulk material.

Outcomes of the proposed fit agree with the signal positions reported by Milošev et al.,[42] who reported C*–P species with a C1s binding energy between 285.8 and 286.2 eV in **ODPA** on a NiTi alloy surface. The obtained atomic concentration ratio [C*–C|C*–H]/[C*–P] equals 18.5, and the expected value is 17. The atomic concentration [C*–C|C*–H] of aliphatic carbon species obtained from the fitting is slightly higher than the expected value. The aspects to assess this difference are the presence of additional substances other than **ODPA**, a non-precise relative sensitive factor ratio of P2p and C1s, and the presence of non-isotropic dried **ODPA** micelles on the sample surface inspected by XPS. O1s spectra were fitted using two contributions based on the obtained binding energy values. The causative oxygen species were identified as P=O* (531.6 eV) and P–O*H with minor contributions from SiO$_2^*$ (533.0 eV). The positions agree with previous studies of **ODPA** on different surfaces.[21,42,43] The expected and obtained atomic concentration

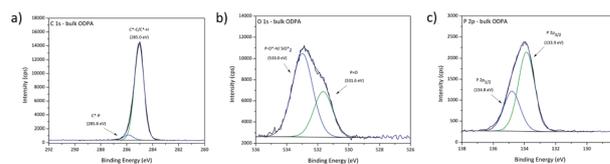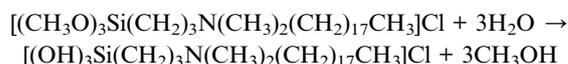**Fig. 2** XPS high resolution spectra for investigated bulk sample **ODPA**, (a) C1s, (b) O1s and (c) P2p signal.

ratio of [P–O*–H]/[P=O*] are both equal two (see Table 2). These results evidence an agreement between the **ODPA** stoichiometry and the proposed fit. The Si2p signal showed the spin–orbit coupling ($\Delta E = 0.6$ eV) from the silicon wafer used as substrate and a peak centred at 103.3 eV from Si*O$_2$ on substrate surface (see Fig. S1a†).[43,44] Based on the fitting, merely 0.16 at% of silicon is in the form of Si*O$_2$. P2p high resolution spectra displayed only the characteristic spin–orbit coupling with an energy distance of 0.93 eV.[45,46] The single P2s peak was centred 57.8 eV higher than the P2p$_{3/2}$ signal, in agreement with the value reported in the literature (see Fig. S1b†).[44]

Concerning the second amphiphilic agent, pure bulk material **DMOAP** is composed of **DMOAP** entities, with the stoichiometry of C$_{26}$H$_{58}$ClNO$_3$Si (see Fig. 1). If a sample of such pure bulk material has a homogeneous composition, the atomic concentrations listed in Table 4 are expected in an XPS investigation based on this stoichiometry. To compare the former with a thick vacuum-dried film, the atomic concentration for a fully hydrolysed **DMOAP** is also listed.

For the water treated **DMOAP**, a hydrolysis of the methoxysilane groups might be expected according to the established behaviour of methoxysilanes with short alkyl chains,[47] as schematically presented below:

$$[(CH_3O)_3Si(CH_2)_3N(CH_3)_2(CH_2)_{17}CH_3]Cl + 3H_2O \rightarrow$$
$$[(OH)_3Si(CH_2)_3N(CH_3)_2(CH_2)_{17}CH_3]Cl + 3CH_3OH$$

This equation is valid for a complete hydrolysis without subsequent condensation. Notably, the process modifies the atomic concentration of carbon in the molecule, and the concentration ratio [C]/[N] can be used as a stoichiometry-based indicator. The [C]/[N] value expected for pristine **DMOAP** is 26, and for homogeneously composed fully hydrolysed **DMOAP** is 23. The respectively observed values are 26.9 and 23.2. Details

Table 3 Ratios between the atomic concentrations of carbon [C], phosphorous [P], and oxygen [O] species, as expected from stoichiometry and found in XPS investigations

Atomic concentration ratio	[C]/[O]	[C]/[P]	[O]/[P]
Expected from stoichiometry	6.0	18.0	3.0
Found by XPS	7.0	19.6	2.8

Table 4 Atomic concentration in at% of the distinct surface species by XPS investigations, compared to stoichiometrically expected values

Sample name	[C]				[O]	[N]			[Si]	[Cl]
	Total	[C*–C/C*–H]	[C*–N$^+$]	[C*–O–Si]	Total	Total	[–N$^+$]	[N*–O]	Total	Total
Bulk **DMOAP**, vacuum-dried	82.21	56.17	14.30	11.74	9.53	3.06	2.61	0.45	2.80	2.40
Expected value for bulk **DMOAP**	81.25	59.37	12.50	9.38	9.36	3.13	3.13	—	3.13	3.13
Water exposed **DMOAP**	80.28	61.33	10.27	8.68	8.73	3.46	3.42	—	4.31	3.22
Expected values for fully hydrolysed **DMOAP**	79.31	65.52	13.79	0	10.34	3.45	3.45	—	3.45	3.45

about the bulk and water exposed **DMOAP** are presented in the C1s high-resolution spectra in Fig. 3 and S3, in the ESI.†

The binding energies of signal contributions from expected species in C1s spectra for bulk **DMOAP** were adjusted based on the carbon covalent binding neighbourhoods and considering the suggested binding energy ranges of the expected binding neighbourhoods as compiled by Beamson and Briggs.[48] Following this, three distinct binding energies for C1s signal contributions were considered, corresponding to aliphatic C*–C/C*–H (285.0 eV), quaternary ammonium-related C*–N$^+$ (286.0 eV), and C*–O in methyl ester groups (286.8 eV) (see Fig. 3). Significant signal contributions from possible carbon species with binding energies higher than 287 eV were not detected.

For a completely hydrolysed **DMOAP** material, a conversion of the C*–O groups is expected, coinciding with a decrease of the atomic concentration of C*–O from the stoichiometrically expected value 9.38 at% or the measured value of 11.74 at% (non-hydrolysed **DMOAP**) to 0 at%. However, for [C*–O] of the water-exposed sample, a value of 8.38 at% was found. The minor changes observed for the surface composition suggest a partial hydrolysis caused by water exposure of the **DMOAP** material after evaporation of the alcoholic solvent. Similarly, the XPS obtained for the thick **DMOAP** film dried and heated at 100 °C in air found small effects on the material composition and, notably, a slight decomposition of methoxy species resulting in a decrease of the [C*–O]/[C*–N$^+$] concentration ratio as presented in Table 5.

Subsequently, structural implications of the spectroscopic outcomes will be highlighted. Considering the stoichiometric composition of **DMOAP**, hydrolysis is expected to be revealed by decreasing the [Si–O*]/[Si*–O] concentration ratio starting from a value of three. The measured value for bulk **DMOAP** agrees with this expected value. After the water treatment, the value reduced to two, indicating a partial oligomerization of **DMOAP** molecules due to a condensation following the partial

hydrolysis of the methoxysilane moieties. However, the C1s peak shape analysis indicates that a substantial portion of the methoxysilane groups were not hydrolysed.

This finding implies that the chemical inertness of the reactive head group of amphiphilic **DMOAP** is attributed to the formation of **DMOAP** micelles in water and to the sterically restricted accessibility of methoxysilane groups for water molecules. Head groups inside micelles may be screened from water by the aliphatic octadecyl tails. Similarly, the formation of ordered structures upon hydrolysis of C_{12}–C_{18} triethoxy(alkyl) silanes was reported by Atsushi et al.[49] Even in acidified solution of ethanol-D6 and deuterated water $CD_3CD_2OD : D_2O$, 80 : 20 w/w, trimethoxysilanes without amino groups and especially trimethoxy (7-octen-1-yl) silane (OEMS) required several hours to present significant hydrolysis, as Brochier-Salon et al. reported.[50]

A covalent attachment of methoxysilane groups to a titania surface requires the formation of a Si–O–Ti bond starting from a hexagonally coordinated Ti centre. Although the formation of Si–O–Ti bridges is established starting from tetrahedrally coordinated tetraalkoxy compounds under sol–gel conditions, the evidence for the formation of Si–O–Ti bonds starting from titania surfaces is based on hydrosilanes or chlorosilanes rather than alkoxysilanes.[40,51,52] Starting from a long-chain alkyl-trialkoxysilane, such as octadecyltriethoxysilane (ODS) on zinc oxide surfaces, the formation of Si–O–Si was reported to dominate the formation of Si–O–Zn bonds, leading to a cross-linked siloxane network that adheres on the substrate surface via hydrogen bonding or with few anchoring points along the surface.[53] Interestingly, acidic properties of both zinc oxide and titania are related to Lewis acid surface sites rather than to Bronsted sites.[52,54] The complexation of the acidic substrate surface sites with oxoanions or esters may be driven by Lewis basic electron pair donor properties of the respective adsorbent providing the oxo-bridge.
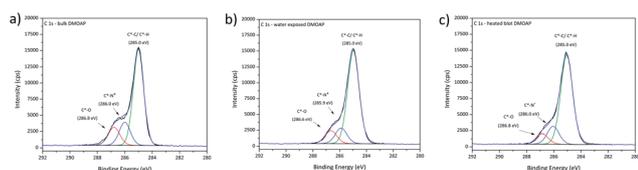

Fig. 3 XPS C1s high-resolution spectra for **DMOAP**, (a) bulk, (b) water exposed, and (c) heated blot.

Table 5 Concentration ratios obtained from fitting C1s signals of **DMOAP** bulk samples prepared following different processes

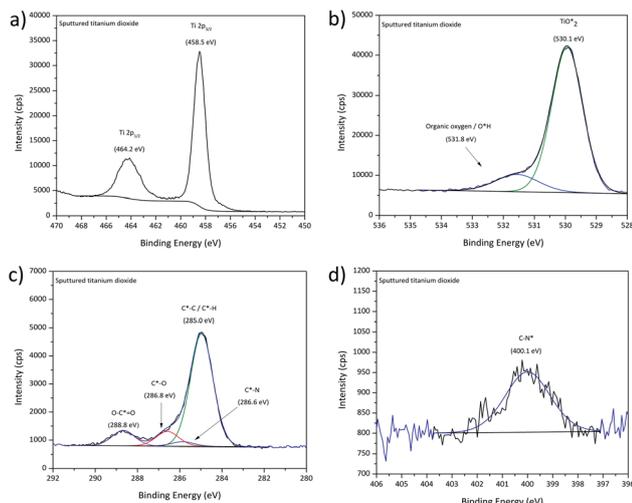| Sample name	[C*–O]/[C*–N$^+$] ratio
Vacuum-dried from solution	0.8
Water exposed	0.8
Thick film after conditioning at 100 °C in air	0.6

Fig. 4 XPS high-resolution spectra for sputtered titanium dioxide, (a) Ti2p, (b) O1s, (c) C1s and (d) N1s signal.

Adsorbed layers on smooth titania substrates

High-resolution XPS spectra of sputter-deposited titanium dioxide are displayed in Fig. 4. The Ti2p spectrum was characterised by one doublet showing a B.E. of 458.5 eV for the $Ti2p_{3/2}$ peak, as expected for titania.[44] The O1s signal presented two contributions attributed to oxidic oxygen from the titanium dioxide centred at 529.9 eV and organic oxygen/hydroxyl groups at 531.6 eV.[21,55] The C1s signal presented four contributions, aliphatic carbon at 285.0 eV, and further contributions at 286.6 eV and 288.7 eV that are also attributed to adventitious carbon in a sorption layer. Finally, in view of the nitrogen

species accompanied by an N1s signal with a binding energy of 400.1 eV, a minor contribution of moieties containing organic nitrogen at 285.9 eV (ref. 21 and 55) was considered.

ODPA/titania films

Films assembled on these substrates from clear **ODPA** formulations were used as reference for a well-ordered monolayer with their structure widely studied over the years on polar oxide surfaces like alumina, silica, or titanium aluminium alloys.[21,43,56] Theile-Rasche et al. recently reported photoelectron spectroscopic peculiarities in C1s spectra of **ODPA** SAMs on $Ti_{0.5}Al_{0.5}N$ hard coatings. Therefore, a more detailed approach for the XPS signal fitting was pursued.[21] As a reference for the C1s and O1s signals of **ODPA**-based assemblies, the spectra obtained for bulk **ODPA** were used. The correspondingly fitted signals of the most relevant studied film samples are displayed in Fig. 5, and further findings are presented in Fig. S3.† For the adsorbate obtained after 4 h immersion and subsequent rinsing with ethanol, the C1s signal displayed in Fig. 5a was dominated by the contribution from aliphatic carbon species (with a binding energy of 285.0 eV) and showed a contribution provided by C*–P bonded carbon atoms.

Comparing the respective spectra obtained for sputter-deposited titania and for the TiO₂/**ODPA** films prepared by 24 h immersion and subsequent rinsing with ethanol (Fig. 5b), there is clear reduction of the carboxylate adsorbed on the surface. However, indications for adventitious carbon species like C*–O (at 286.6 eV) and carboxylates (at 288.7 eV) were still observed as well as a contribution of organic nitrogen at 285.9 eV.[21,55] The O1s signal presented two contributions with the peaks centred at 529.9 eV and 531.6 eV (Fig. 5c and d). This

Table 6 Normalized XPS signal intensity ratios for **ODPA** samples adsorbed on titania, based on the sample immersed for 24 h in ethanolic **ODPA** solution and then rinsed with ethanol (subsequently labelled "SAM"), and estimated layer thickness

Sample name	{[P]/[Ti]}/{[P]/[Ti]}$_{SAM}$	{[C]/[P]}/{[C]/[P]}$_{SAM}$	Estimated layer thickness (nm)
TiO₂/**ODPA** 4 h EtOH	0.58	0.47	0.4
TiO₂/**ODPA** 24 h EtOH	1.00	1.00	1.5
TiO₂/**ODPA** 72 h EtOH	1.00	0.88	1.3
Bulk **ODPA**	—	0.71	> 10

Table 7 Atomic concentration in at% of the distinct surface species from XPS investigations of **DMOAP**/titania films

|	[C]					[O]		[N]			[Si]	[Ti]	[Cl]
Sample name	[C*–C/C*–H]	[C*–N⁺]	[C*–O]	[C*–N]	[O–C*=O]	[TiO₂*]	[Organic oxygen/ O*H]	[Si–O*]	[C–N*]	[–N⁺]	[O₃Si*–C]	[Ti*O₂]	[Cl⁻]
TiO₂/**DMOAP**-A 10 min heated	25.04	3.25	2.29	0.75	2.38	36.38	6.82	1.09	0.76	0.84	1.85	17.64	0.47
TiO₂/**DMOAP**-N 10 min heated	18.71	2.43	1.55	0.65	2.04	41.35	7.53	0.86	0.61	0.62	1.27	12.22	0.00
TiO₂/**DMOAP**-N 24 h heated	36.85	1.66	3.19	1.10	2.64	27.91	5.40	3.98	1.05	0.43	2.47	13.22	0.08
TiO₂/**DMOAP**-N 24 h	38.56	1.54	4.13	1.35	3.70	22.84	5.12	6.60	1.35	0.41	1.63	12.22	0.00
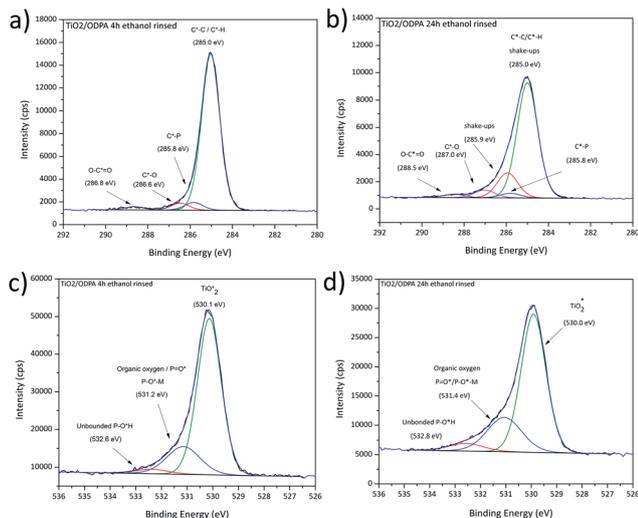
Fig. 5 High-resolution C1s and O1s XPS spectra obtained for ODPA layers on titania after immersion in ODPA solution for 4 h (a) and (c); 24 h (b) and (d).
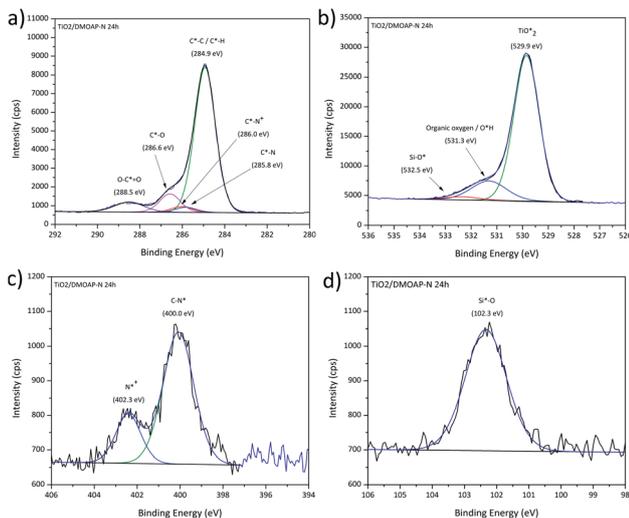

Fig. 6 XPS high-resolution spectra for DMOAP layer on titania, (a) C1s, (b) O1s, (c) N1s and (d) Si2p signals.

indicates a partial competitive desorption of adventitious carbon moieties due to the formation of specifically adsorbed **ODPA** films. However, a thorough replacement of adsorbed carboxylate species was observed only after considerably longer

immersion periods. In detail, when the immersion time was increased from 4 h to 24 h, a significant raise of the **ODPA** coverage on titania by approximately 70% (as shown in Table 6) was found; however increasing the immersion time to 72 h did not result in a further raise of the **ODPA** surface coverage. Additionally, the increase of the layer thickness reached a maximum value of 1.5 nm, consistent with a monolayer formation.[57] Along with the compaction of the **ODPA** layers when extending the exposure in **ODPA** solution to 24 h, the C1s signal became wider and asymmetric, displaying additional features, as depicted in Fig. 5b. These spectral features, as shown in Fig. 5b, may be related to vibrational shake-ups. This observation is consistent with the formation of a self-assembled monolayer structure, as reported by Theile-Rasche et al.,[21] who suggested components at 285.4, 285.8, and 286.4 eV due to vibrational shake-ups similar to the ones reported for polyethylene.

In contrast to **ODPA** adsorbates rinsed with ethanol, the film surfaces of equally immersed but water rinsed **ODPA**/titania specimens presented a signal shape similar to the investigated **ODPA** bulk sample indicating the presence of physisorbed **ODPA** species on the surface of the assembled layer.

Following the applied XPS-based strategy for assessing details related to the bonding situation of the adsorbed species, the O1s spectral region was investigated in more detail. Aside from the two peaks fitted to encompass the contributions in case of the pristine titania, the O1s high-resolution signals obtained for thicker water-rinsed **ODPA** films revealed a further spectral and, thus, chemical feature contributing to a third peak at a higher binding energy around 532.7 eV, as presented in Fig. 5c and d. The concentration ratio [P=O*]/[P–O*H] did not agree with the value of 0.5 found for bulk **ODPA**. This finding may be due to remaining water trapped close to the polar titania substrate surface or to contributions from the phosphonate species in the underlying **ODPA**/titania monolayer. Both discussed samples presented a peak at 530.0 and 530.1 eV due to oxidic oxygen species from titania, which indicates that contributions from the film/substrate interphase were also recorded. The second contribution centred at 531.1–531.4 eV is attributed to organic oxygen, P=O* and P–O*–metal ion bonds.[21,42,55] In prior studies of films formed from phosphonic acids, contributions resulting in O1s peaks with higher binding energies than 532 eV were tentatively attributed to unbonded phosphonic acid P–O*H groups.[21] A lower surface concentration from unbound groups suggests the presence of physisorbed

Table 8 Normalized atomic concentration ratios for freshly prepared DMOAP films on titania surfaces as obtained by XPS and referencing the findings for the DMOAP-N/titania films obtained after 24 h immersion (labelled "DMOAP-N 24 h" here)

Sample name	{[Si]/[Ti]}/{ [Si]/[Ti]}DMOAP-N 24 h	{[C]/[Si]}/{ [C]/[Si]}DMOAP-N 24 h	Estimated layer thickness (nm)
TiO2/**DMOAP**-A 10 min heated	0.8	0.6	0.9
TiO2/**DMOAP**-N 10 min heated	0.8	0.6	0.6
TiO2/**DMOAP**-N 24 h	1.0	1.0	1.8
TiO2/**DMOAP**-N 24 h heated	1.4	0.6	1.7
Bulk **DMOAP** vacuum dried	—	1.0	—

Table 9 Contact angle results for DMOAP and ODPA films on smooth titania (freshly prepared)

Sample name	Water contact angle (°)
TiO$_2$	11.4 ± 3.5
TiO$_2$/DMOAP-N 10 min	80.0 ± 0.9
TiO$_2$/DMOAP-A 10 min	86.8 ± 0.9
TiO$_2$/DMOAP-N 10 min heated	65.1 ± 0.8
TiO$_2$/DMOAP-A 10 min heated	63.1 ± 3.0
TiO$_2$/DMOAP-N 24 h	82.3 ± 2.5
TiO$_2$/DMOAP-A 24 h	85.4 ± 0.4
TiO$_2$/DMOAP-N 24 h heated	48.8 ± 1.1
TiO$_2$/DMOAP-A 24 h heated	48.3 ± 0.4
TiO$_2$/ODPA, 4 h EtOH rinsed	99.5 ± 0.5

octadecylphosphonic acid. However, the ODPA/titania film obtained after 24 h of immersion and subsequent ethanol rinsing still exhibited a high-binding energy contribution in the O1s spectrum. As AFM investigations of this sample surface did not reveal significant rises, such as patches or physisorbed ODPA micelles (as shown in Fig. 8). This finding may indicate that the chemisorbed ODPA is attached to the surface through tri and bidentate bounds rather than mono-dentate. Similar XPS findings were not detailed by Theile-Rasche *et al.*, which may be due to the intense O1s signal contributions of the mixed oxide layer of the Ti$_{0.5}$Al$_{0.5}$N coating they investigated. Due to the predominance of a mono-dentate conformation, a higher contribution of unbound groups may be expected, leading to similar O1s contributions, as observed for the investigated bulk ODPA specimen. The observed P2p$_{3/2}$ binding energy is consistent with the values reported for immobilized phosphonates in the literature (see Fig. S3 and S4†).[46,58]

DMOAP/titania films

The XPS findings for the investigated DMOAP/titania films are summarised in Table 7, displaying the detected elements and the contributions of the attributed chemical species.

The fitting procedures applied to the spectrum sets of all samples were based on those used for the pristine titania and the bulk DMOAP samples. The binding energy positions observed for all adsorbate signals, in case of all samples, are consistent with the species expected for an adsorbed layer of DMOAP.[21,48,55] High-resolution Si2p spectra for all the considered DMOAP/titania samples included a centrosymmetric peak with a binding energy between 101.5 and 102.3 eV (see Fig. 6d and S5†), consistent with the presence of groups with a –C–SiO$_3$– binding environment of the silicon atoms on the surface.[59,60] N1s spectra are presented in detail in Fig. 6. Compared to pristine titania, DMOAP/titania exhibited an additional peak at higher binding energy, consistent with the presence of quaternary ammonium according to the species of the carbon signal, and with the bulk sample.[20,60,61] There is no significant difference between the shapes on the acidified and the neutral medium, not even on the heated and unheated samples. The C1s high-resolution spectrum of the sample immersed for 24 h is displayed in Fig. 6a. The peak with a binding energy of 286.0 eV is attributed to contributions from C*–N$^+$ species. In the frame of the fitting procedure, an area constraint was applied for this contribution to ensure a reasonable value based on DMOAP stoichiometry showing a C$_4$N$^+$ binding environment.

Remarkably, the C1s signal for all these samples revealed contributions around 288.5 eV, attributed to carboxylate species. Following the rationale established for ODPA/titania films, this finding indicates that the DMOAP species do not competitively adsorb on the titania surface to form a chemisorbed monolayer structure. Moreover, C1s shake-up contributions, as observed for the ODPA/titania monolayers, were not found. Three species were detected in the O1s spectra for all samples, as illustrated in Fig. 6b. The contribution centred at approximately 532.5 eV is due to Si–O* bounds, consistent with the Si2p signal and the findings for DMOAP bulk samples.[48,55,62] Although the samples prepared in different medium show

Table 10 Mean (SD) findings of *E. coli* growth attached to sample surface in 24 h[a]

Treatment group	Time evaluation		
	Initial	Maximum	Final
TiO$_2$	0.099 (0.2 × 10^{-2}) Ca	0.442 (0.03) Ab	0.287 (0.07) Bb
TiO$_2$/DMOAP-A 10 min	0.100 (0.6 × 10^{-2}) Ca	0.445 (0.05) Ab	0.346 (0.03) Bab
TiO$_2$/DMOAP-A 10 min heated	0.102 (0.7 × 10^{-2}) Ca	0.491 (0.03) Aab	0.394 (0.03) Bab
TiO$_2$/DMOAP-A 24 h	0.096 (0.07 × 10^{-2}) Ba	0.512 (0.03) Aa	0.430 (0.06) Aa
TiO$_2$/DMOAP-A 24 h heated	0.101 (0.5 × 10^{-2}) Ca	0.460 (0.05) Ab	0.334 (0.5 × 10^{-2}) Bab
TiO$_2$/DMOAP-N 10 min	0.098 (0.09 × 10^{-2}) Ca	0.494 (0.02) Aab	0.356 (0.03) Bab
TiO$_2$/DMOAP-N 10 min heated	0.096 (1.1 × 10^{-2}) Ca	0.481 (0.01) Aab	0.360 (0.04) Bab
TiO$_2$/DMOAP-N 24 h	0.104 (1.1 × 10^{-2}) Ca	0.545 (0.04) Aa	0.413 (0.06) Bab
TiO$_2$/DMOAP-N 24 h heated	0.099 (0.4 × 10^{-2}) Ca	0.454 (0.05) Ab	0.353 (0.02) Bab
TiO$_2$/ODPA	0.102 (1.1 × 10^{-2}) Ca	0.461 (0.04) Ab	0.338 (0.02) Bab
p-value	*p* = 0.826	*p* = 0.026	*p* = 0.016

[a] Mean values followed by distinct letters differ statistically at 5%, according to two-way repeated measures ANOVA and Bonferroni test. Uppercase letters compare time evaluation within treatment group (lines). Lowercase letters compare treatment groups (columns).
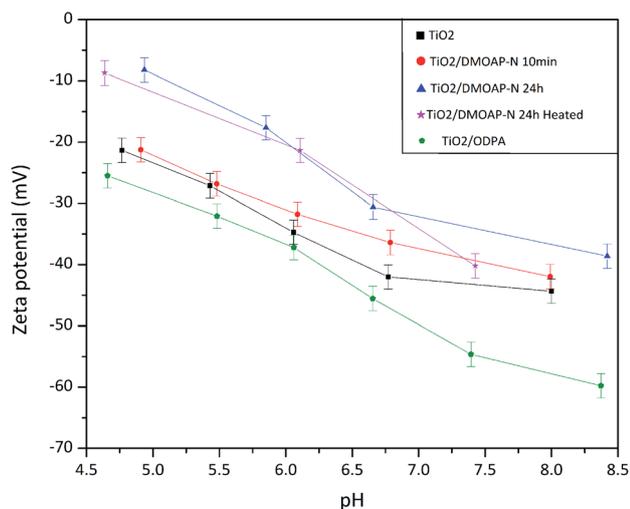
Fig. 7 Zeta potential results for the studied layers on smooth titanium dioxide.
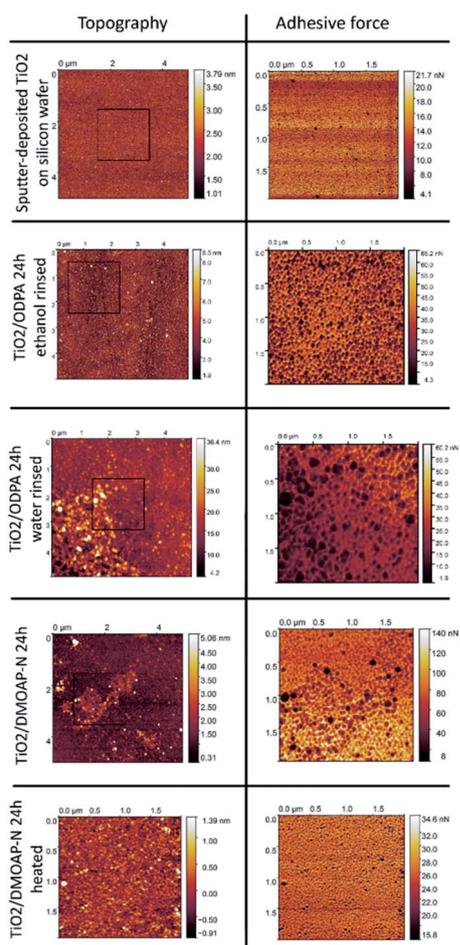

Fig. 8 AFM height and adhesion force image for the investigated layers.

similar signal shapes, the silanol contribution clearly increased after the heat treatment along with a decrease of the contact angle, as presented in Table 9.

In Table 8, the estimated layer thickness and different ratios for the investigated samples normalized for the TiO_2/**DMOAP**-N 24 h sample are displayed. Heating a film in air at 100 °C did not modify the film thickness. However, the normalised [C]/[Si] ratio was affected by performing the annealing process. This is highlighted for the TiO_2/**DMOAP**-N 24 h sample. On the one hand, the [C]/[Si] found for the dried sample was equal to the respective ratio of the bulk sample. This is attributed to the absence of a preferential molecular orientation perpendicular to the sample surface in both cases. On the other hand, the heated film sample showed a considerably decreased [C]/[Si] concentration ratio. This result indicates that the annealing procedure induces a preferential orientation, which leads to higher exposure of the silanol groups close to the film surface. The concomitant increase of the [Si]/[Ti] ratio is in concordance with modification of this layer.

As XPS is a surface-sensitive technique and some preferential molecular orientation may introduce a nanoscale structural anisotropy in films, these findings may be expected to sensitively reflect such geometric effects. Therefore, the difference found between the signal intensities of the heated and unheated samples, which were coated in concordant processes establishing coincident surface coverages, suggests that the heat treatment rearranges the adsorbed layer.

Comparing ODPA/titania and DMOAP/titania films

Finally, in the headgroup densities of **ODPA**/titania and **DMOAP**/titania films prepared by 24 h immersion in alcoholic solutions and subsequent rinsing with ethanol, the [Si]/[Ti] concentration ratio amounting to 0.14 is 1/3 higher than the [P]/[Ti] concentration ratio for the **ODPA** monolayer. In addition to the strong headgroup attachment facilitating competitive desorption of carboxylic adventitious carbon species and the highly ordered film structure resulting in C1s shake-ups, this finding substantiates that although these films exhibit similar thickness their assembly schemes have significant differences. This is also reflected when considering the respective differences with respect to the surface concentrations of the bulk samples, revealed by values around 1 and 0.6 for $\{[C]/[Si]\}_{bulk}/\{[C]/[Si]\}_{DMOAP\text{-}N,24\ h}$ and $\{[C]/[P]\}_{bulk}/\{[C]/[P]\}_{SAM}$, respectively. Evaluating the relative XPS signal contributions from atoms in head and tail group for bulk or film specimens, respectively, may be considered an effective approach to find orientational differences of amphiphilic species in the distinctly assembled phases.

Contact angle measurements

The layer modification can be noticed also by the decrease of the water contact angle after the heating procedure (as shown Table 9). Since **DMOAP** and **ODPA** have long alkyl chain (octadecyl tails) and a minor solubility in water, the presence of the adsorbates on the surfaces can be verified by contact angle measurements. Surfaces terminated by methylene $–CH_2$ and methyl $–CH_3$ groups were reported to present a water contact angle (WCA) higher than 90°.[63] Nonetheless, immediately after its preparation and a few minutes in contact with ambient air
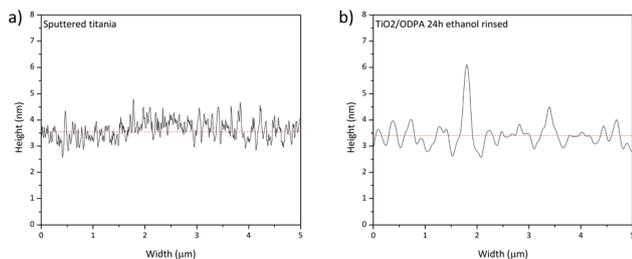
Fig. 9 AFM height profile of (a) sputtered titanium dioxide and (b) ODPA monolayer.

Fig. 10 *S. mutans* growth after exposition to different samples during three different periods.

Table 11 Changes of water contact angles obtained for thick and thin **DMOAP** films on titania substrates and for **ODPA**/titania after 24 h exposure to bacterial medium containing *S. mutans* and subsequent rinsing with alcohol

Sample name	Water contact angle (°)
Before rinsing in isopropanol	92.8 ± 8.3
After rinsing in isopropanol	54.2 ± 8.4
After 1 h exposition in biological medium	65.4 ± 16.1
After 4 h exposition in biological medium	58.9 ± 12.3
After 24 h exposition in biological medium	55.2 ± 23.5
TiO_2/**DMOAP**-N 24 h heated	46.3 ± 4.2
TiO_2/**ODPA** 4 h	88.6 ± 8.3

the sputter-deposited titania displayed a low WCA. Thus, for both **DMOAP** and **ODPA** films on titania, a significant increase is expected in the contact angle due to these amphiphiles

adsorption. The results of measured contact angle for the freshly prepared titania and the films after the adsorption of **DMOAP** and **ODPA** are summarized in Table 9.

The observed increase of the WCA for the **ODPA** and **DMOAP**-N 24 h films on titania indicated that the surface is mainly terminated by $–CH_2$ and $–CH_3$ groups.[63] Such effect of film formation was corroborated by the XPS results, which were obtained after 24 h immersion of titania substrates in **ODPA** or **DMOAP** containing formulations, and indicate the presence of aliphatic carbonaceous species on the surface. The contact angle strongly decreased due to the heating procedure indicating an alteration of the adsorbed layer, as presented in Table 8.

Such modifications are comparable to the results presented by D'Elia *et al.*,[63] who demonstrated the influence of the film formation temperature on the thickness and contact angle of **DMOAP** layers on oxidic ITO thin films. After the heat treatment at 120 °C, the contact value was near 67°, and similar results were obtained in our study. Following a heat treatment at 100 °C, the WCA findings displayed in Table 10 were 64° for samples immersed for 10 minutes and 48° for samples immersed for 24 hours. D'Elia *et al.* explained the contact angle reduction in the case of **DMOAP**/ITO films due to a disordering of the **DMOAP** layer induced by the heat treatment. Those authors stated that lower drying temperatures (about 85 °C) are suitable for the formation of ordered **DMOAP** monolayers.

The measured WCA value for the **ODPA** layer presented in Table 9 agreed with the literature and indicated the presence of a layer on TiO_2 surface. Chen *et al.* reported a WCA between 90° and 110° according to the concentration of **ODPA** adsorbed on aluminium.[64] Further studies also showed water contact angles higher than 100° for adsorbed ordered **ODPA**.[22,56]

Zeta potential measurements

Zeta potential investigations are mainly performed on colloidal suspensions of different materials.[65] In this case, different factors can modify the zeta potential values and the isoelectric point; for instance, the particle size, roughness, and crystalline phase of materials prevailing in distinct modifications, such as titania.[66,67] Besides the investigation of differently modified titania surfaces, the approach presented in this work was done using a smooth substrate to avoid the influence of roughness on the measurement. Thus, the results are mostly influenced by the adsorbed species on the surface.

The results of these measurements are displayed in Fig. 7. Pristine titania samples presented a plateau between pH 6.0 and 8.0. Ferraris and co-workers who investigated different Ti6Al4V surfaces reported similar results for a chemically treated sample.[65] The occurrence of such plateau was attributed by Ferrari *et al.* to the presence of acid hydroxyl groups. The OH groups terminating the titania surface were also revealed by the XPS findings, reinforcing this explanation as presented in Fig. 4. The zeta potential results displayed in Fig. 7 show, apart from the **DMOAP**/titania sample immersed for 10 minutes, an increase of the zeta potential after adsorption of **DMOAP**. Although it is difficult to quantitatively compare trends of zeta potential measurements obtained for samples in such different

geometries as powders and films, in this study, a zeta potential shift towards more positive values was also observed for quaternary ammonium-containing molecules adsorbed on membranes compared to bare membranes.[68–70] Such shift caused by the presence of quaternary ammonium agrees with the XPS outcomes that showed the presence of C–N$^+$ in **DMOAP**/titania films obtained after immersion in **DMOAP** solution. Moreover, as presented in Fig. 7, **ODPA** adsorbed on titania shifted towards lower zeta potential values, in qualitative agreement with reported studies of **ODPA** adsorbed on different materials.[71,72] The shift of the zeta potential at basic pH was possibly due to unbonded P–OH groups, which will be investigated in more detail.

AFM investigations

The layers obtained by self-assembly of **ODPA** and adsorption of **DMOAP** on the surface of sputter-deposited titania films on flat and smooth silicon wafers were investigated by AFM and evaluated in comparison with the pristine substrate. The surface root mean square (RMS) R_q of the surface roughness obtained by AFM for TiO$_2$/Si film was 0.41 nm. As illustrated in Fig. 8, the surface of an uncoated TiO$_2$/Si substrate revealed a homogeneous and smooth topography characterized by imaged height differences with the range of up to 3 nm. Upon interaction with the AFM tip, the most pronounced risings with heights around 3 nm exhibit distinct adhesion properties, from the surrounding smooth substrate areas, and are attributed to particulate deposits.

Subsequently, we assessed the microscopically characterized surface properties achieved by 24 h of immersion in alcoholic solutions of separate amphiphiles **ODPA** or **DMOAP** and subsequent sample conditioning steps with distinct rinsing or mild heating procedures.

After immersion in **ODPA**-containing ethanolic solutions and subsequent rinsing with the solvent, the obtained TiO$_2$/**ODPA** sample displayed height differences with a range of up to 7 nm and a R_q roughness of 1.1 nm. The most pronounced risings with heights around 7 nm had distinct adhesion properties from the surrounding smooth substrate areas. As their areal density is higher than that of the pristine substrates, they are attributed to particulate deposits obtained during the process chain comprising immersion and rinsing steps.

In contrast, when rinsed with water after the immersion, an increased R_q roughness, around 4.2 nm was observed along with patch-like deposits with a width of approximately 0.1 μm. On the upper right area, the R_q was 2.4 nm, and on the lower left area, 6.7 nm. The differences in topography and adhesion properties as compared to the pristine substrate surfaces are attributed to the formation of adsorbates and to local deposition of surplus organic material. For its areal density, less than 10% of the imaged surface area is significantly lower when rinsed with ethanol than that exposed to water during rinsing. After immersion in **DMOAP**-containing ethanolic solutions and subsequent rinsing with the water, the obtained TiO$_2$/**DMOAP**-N sample showed height differences up to 2 nm and a R_q roughness of 0.35 nm.

After immersion in **DMOAP**-containing ethanolic solutions and subsequent rinsing with water, the obtained TiO$_2$/**DMOAP**-N sample displayed height differences up to 2 nm and a R_q roughness of 0.35 nm. After the sample was exposed to a heating process at 100 °C in air overnight, the obtained TiO$_2$/**DMOAP** heated samples revealed an increase in roughness of 0.69 nm and imaged height differences up to 5 nm. The findings obtained by SFM investigations of **ODPA**/titania films along with the XPS results indicate the formation of **ODPA**/titania SAMs after rinsing with ethanol and the deposition of thicker **ODPA**/titania films composed of octadecylphosphonic acid on top of an **ODPA**/titania SAM when rinsed with water instead. For the thin **DMOAP**/titania film, the roughening of the film surface and the occurrence of elevated patch regions with distinctive adhesion properties are interpreted to result from the thermal conditioning process.

Fig. 9 presents the height profile for sputtered titania and the SAM of **ODPA**. The profile shows a difference caused by the physisorbed **ODPA** species on the surface of the assembled layer, consistent with the aforementioned discussion. This finding may point to **ODPA** micelles on the SAM surface. The formation probably occurred during the washing procedure because **ODPA** is only poorly soluble in water. Such geometric film model explains the occurrence of approximately 5 nm height nanoscale risings as observed in the AFM images presented in Fig. 9.

Antibacterial assays

Antibacterial assays were performed to evaluate how the studied samples respond to bacterial agents. In the antibacterial assay against *S. mutans*, the thick DMOAP bulk film presented greater antibacterial activity than the other investigated specimens, which became evident mainly after 24 hours Fig. 10).

To check the efficacy of the prepared surface modified titania samples in longer exposure, adsorbed layers of **ODPA** and **DMOAP** were submitted to a test using *E. coli* for 24 hours. The statistical analysis is displayed in Table 10. All groups showed the same pattern: low growth at the beginning and an intermediate growth in the end of the evaluated time. No surface treatment provided an effective reduction of the bacteria growth compared to the control (TiO$_2$). The TiO$_2$/**DMOAP**-A 24 h group had a more pronounced bacteria growth than the control, which was not expected. The value p is lower than 0.05 for the maximum and final time, showing that the samples are significantly different, but not due to the reduction of the bacteria, as aforementioned. A decrease in bacteria growth was not observed compared to the control.

Although **DMOAP** antibacterial properties have been reported in different studies, there was a strong modification on the surface wettability after the biological assay, indicating that during the incubation period **DMOAP** layers are partially removed. This statement is based on the water contact angle measurements presented in Table 11 that reveal the changes of the WCA during the antibacterial test.

Notwithstanding, different characterization, *e.g.* by zeta potential measurements requiring test periods of approximately

one hour, indicated the immobilization of **DMOAP** on the titania surfaces. However, the adsorbed layer appears strongly affected by the biological assay and is possibly released to the biological medium. Such finding suggests that following the applied immobilization scheme, the resulting **DMOAP** layers are significantly less stable than the assembled **ODPA** layers, although covalent attachment on the titania surface may be anticipated for both adsorptives. As the thick **DMOAP** bulk film presented the higher antibacterial activity, the activity could be influenced by the adsorbate mobility and/or release. Accordingly, Štular and co-workers reported that after several washing procedures, **DMOAP** was partially removed from cotton surface.[73] The release of alkylorganosilanes was reported by Torun and co-workers, who revealed that alkylorganosilanes anchor by few points on ZnO surface leading to a small number of covalent bonds.[53] Thereby, well ordered **DMOAP** monolayers might not be suitable for antibacterial coatings since the quaternary ammonium groups are not easily accessed by the bacteria membrane.

Conclusions

The presented study aimed at providing a comprehensive experimental setup with distinct methods and scales for promoting a systematic characterization of octadecylphosphonic acid (**ODPA**) and dimethyloctadecyl[3-(trimethoxysilyl) propyl] ammonium chloride (**DMOAP**) adsorbed on smooth or structured surfaces to deliver new information about the structure–property relationships accompanying the surface modification. By applying the proposed methodology, new details were provided for the immobilization and assembly of such adsorptives on titania surfaces, starting from films on smooth oxide surfaces. The choice of the substrates provides access to physicochemical properties of such structures, which minimizes the substrate influence. **ODPA** and **DMOAP** on sputter-deposited titania were intensively characterized through different techniques. XPS characterization was performed starting from the bulk materials. After the adsorption of **ODPA** on titania for 24 hours of immersion and subsequent rinsing with ethanol, the C1s high-resolution spectra showed contributions consistent with a monolayer formation, presenting decrease of carboxylate on the surface. Such structure was only observed in samples prepared during longer immersion periods followed by washing with the same solvent, confirming that time and rinsing procedures play a crucial role in monolayer formation. The layer thickness of 1.5 nm reinforces the presence of a monolayer.

Well-ordered and strongly attached monolayers were not observed for distinct approaches of assessing **DMOAP** adsorbed on smooth titania, although different characterization indicated the presence of a layer on the surface. XPS and zeta potential measurements verified the presence of quaternary ammonium groups close to the surface. The mild heat treatment for conditioning **DMOAP** layers promoted a reorganization of the constituents of the films on the surface but did not significantly attach the reactive trimethoxysilyl headgroups to the titania substrate. The complete hydrolysis of trimethoxysilyl

moieties was identified as a challenge for the synthesis of bioactive films from dispersions composed of functional amphiphilic molecules. Congruently, sample surface characterization after the biological assays found that **DMOAP** layers are not stable after one day of exposure to aqueous media and could be released during the test. The fact that a several micrometres thick **DMOAP** film presented the highest antibacterial activity against Gram-positive *S. mutans* bacteria could be due to release from an imperfectly attached and crosslinked film and the mobility of the thus dispersed species in the bacterial medium. Thus, the preparation plays a crucial role in the activity of **DMOAP** layers, and a thin layer would not be suitable for an extended antibacterial activity. Likewise, the results showed that the protocols reported in the literature cannot be applied for titania surfaces.

The proposed methodology elucidates aspects of bioactive layers on titania based on the structure of the adsorbents on the surface, providing physicochemical characterization of the layers before and after biological assays. Such approach could also be applied to other bioactive layers on variably coated substrates to provide new information about the layer properties rather than only biological activities.

Conflicts of interest

The authors declare that they do not have any conflicts of interest.

Acknowledgements

Notes and references

1 Q. Wei, S. Krysiak, K. Achazi, T. Becherer, P. L. M. Noeske, F. Paulus, H. Liebe, I. Grunwald, J. Dernedde, A. Hartwig, T. Hugel and R. Haag, *Colloids Surf. B Biointerfaces*, 2014, **122**, 684–692.

2 K. Stapelfeldt, S. Stamboroski, I. Walter, N. Suter, T. Kowalik, M. Michaelis and D. Brüggemann, *Nano Lett.*, 2019, **19**, 6554–6563.

3 Y. R. Corrales-Ureña, Z. Souza-Schiaber, P. N. Lisboa-Filho, F. Marquenet, P. L. Michael Noeske, L. Gätjen and K. Rischka, *RSC Adv.*, 2019, **10**, 376–386.

4 K. Borcherding, D. Marx, L. Gätjen, N. Bormann, B. Wildemann, U. Specht, D. Salz, K. Thiel and I. Grunwald, *Materials*, 2019, **12**, 1–13.

5 E. S. Bronze-Uhle, L. F. G. Dias, L. D. Trino, A. A. Matos, R. C. de Oliveira and P. N. Lisboa-Filho, *Surf. Coating. Technol.*, 2019, **357**, 36–47.

6 J. Meng, X. Zhang, L. Ni, Z. Tang, Y. Zhang, Y. Zhang and W. Zhang, *Desalination*, 2015, **359**, 156–166.

7 K. Zhang, Y. Zhu, X. Liu, Z. Cui, Y. Xianjin, K. W. K. Yeung, H. Pan and S. Wu, *Mater. Des.*, 2017, **130**, 403–412.

8 X. Zhang, L. Wang and E. Levänen, *RSC Adv.*, 2013, **3**, 12003–12020.

9 H. Braunwarth and F. H. H. Brill, *Wound Med*, 2014, **5**, 16–20.

10 J. L. Grace, J. X. Huang, S. E. Cheah, N. P. Truong, M. A. Cooper, J. Li, T. P. Davis, J. F. Quinn, T. Velkov and M. R. Whittaker, *RSC Adv.*, 2016, **6**, 15469–15477.

11 R. Kaur and S. Liu, *Prog. Surf. Sci.*, 2016, **91**, 136–153.

12 P. Dogra, R. Dharela, G. S. Chauhan, R. Gupta and W. Azmi, *Procedia Chem.*, 2012, **4**, 208–215.

13 P. Elena and K. Miri, *Colloids Surf. B Biointerfaces*, 2018, **169**, 195–205.

14 J. M. Antonucci, D. N. Zeiger, K. Tang, S. Lin-Gibson, B. O. Fowler and N. J. Lin, *Dent. Mater.*, 2012, **28**, 219–228.

15 R. S. Boethling, *Water Res.*, 1984, **18**, 1061–1076.

16 T. R. Neu, *Microbiol. Rev.*, 1996, **60**, 151–166.

17 J. J. H. Oosterhof, K. J. D. A. Buijssen, H. J. Busscher, B. F. A. M. Van Der Laan and H. C. Van Der Mei, *Appl. Environ. Microbiol.*, 2006, **72**, 3673–3677.

18 L. A. T. W. Asri, M. Crismaru, S. Roest, Y. Chen, O. Ivashenko, P. Rudolf, J. C. Tiller, H. C. Van Der Mei, T. J. A. Loontjens and H. J. Busscher, *Adv. Funct. Mater.*, 2014, **24**, 346–355.

19 K. Belkhir, M. Lacroix, M. Jamshidian, S. Salmieri, C. Jegat and M. Taha, *Food Packag. Shelf Life*, 2017, **12**, 28–41.

20 W. He, Y. Zhang, J. Li, Y. Gao, F. Luo, H. Tan, K. Wang and Q. Fu, *Sci. Rep.*, 2016, **6**, 1–9.

21 C. Theile-Rasche, M. Wiesing, S. Schwiderek, M. Noeske and G. Grundmeier, *Appl. Surf. Sci.*, 2020, **513**, 145701.

22 C. Dai, N. Liu, Y. Cao, Y. Chen, F. Lu and L. Feng, *Soft Matter*, 2014, **10**, 8116–8121.

23 M. W. Kulka, I. S. Donskyi, N. Wurzler, D. Salz, Ö. Özcan, W. E. S. Unger and R. Haag, *ACS Appl. Bio Mater.*, 2019, **2**, 5749–5759.

24 H. Fabre, D. Mercier, A. Galtayries, D. Portet, N. Delorme and J. F. Bardeau, *Appl. Surf. Sci.*, 2018, **432**, 15–21.

25 E. Al-Zaidi and X. Fan, *Colloid. Surface. Physicochem. Eng. Aspect.*, 2018, **543**, 1–8.

26 K. M. F. Rossi de Aguiar, V. S. Alves, P.-L. M. Noeske, K. Rischka, M. B. Portela, A. Ferreira-Pereira and U. P. Rodrigues-Filho, *Hybrid films based on nonisocyanate polyurethanes with antimicrobial activity*, 2019.

27 Y. R. Corrales Ureña, L. Wittig, M. Vieira Nascimento, J. L. Faccioni, P. N. Lisboa Filho and K. Rischka, *Appl. Adhes. Sci.*, 2015, **3**, 7.

28 C. Adlhart, J. Verran, N. F. Azevedo, H. Olmez, M. M. Keinänen-Toivola, I. Gouveia, L. F. Melo and F. Crijns, *J. Hosp. Infect.*, 2018, **99**, 239–249.

29 L. H. Hsu, D. Kwaśniewska, S. C. Wang, T. L. Shen, D. Wieczorek and Y. L. Chen, *Sci. Rep.*, 2020, **10**, 1–12.

30 M. E. Forman, M. C. Jennings, W. M. Wuest and K. P. C. Minbiole, *ChemMedChem*, 2016, **11**, 1401–1405.

31 A. Camposeo, O. M. Maragò, B. Fazio, B. Klöter, D. Meschede, U. Rasbach, C. Weber and E. Arimondo, *Appl. Phys. B Lasers Opt.*, 2006, **85**, 487–491.

32 Y. Jiao, L. Niu, S. Ma, J. Li, F. R. Tay and J. Chen, *Prog. Polym. Sci.*, 2017, **71**, 53–90.

33 S. Pletincx, L. L. I. Fockaert, J. M. C. Mol, T. Hauffman and H. Terryn, *npj Mater. Degrad.*, 2019, **3**, 1–12.

34 J. Liu, C. Du, H. T. Beaman and M. B. B. Monroe, *Pharmaceutics*, 2020, **12**, 419–436.

35 A. A. Torkelson, A. K. da Silva, D. C. Love, J. Y. Kim, J. P. Alper, B. Coox, J. Dahm, P. Kozodoy, R. Maboudian and K. L. Nelson, *J. Appl. Microbiol.*, 2012, **113**, 1196–1207.

36 J. E. Sader, R. Borgani, C. T. Gibson, D. B. Haviland, M. J. Higgins, J. I. Kilpatrick, J. Lu, P. Mulvaney, C. J. Shearer, A. D. Slattery, P. A. Thorén, J. Tran, H. Zhang, H. Zhang and T. Zheng, *Rev. Sci. Instrum.*, 2016, **87**, 093711–093714.

37 J. S. Villarrubia, *Surf. Sci.*, 1994, **321**, 287–300.

38 F. Mangolini, J. B. McClimon, F. Rose and R. W. Carpick, *Anal. Chem.*, 2014, **86**, 12258–12265.

39 H. Li, H. Bao, K. X. Bok, C. Y. Lee, B. Li, M. T. Zin and L. Kang, *Biomater. Sci.*, 2016, **4**, 299–309.

40 E. P. Ferreira-Neto, S. Ullah, M. B. Simões, A. P. Perissinotto, F. S. de Vicente, P. L. M. Noeske, S. J. L. Ribeiro and U. P. Rodrigues-Filho, *Colloid. Surface. Physicochem. Eng. Aspect.*, 2019, **570**, 293–305.

41 C. Tornow, P. L. M. Noeske, S. Dieckhoff, R. Wilken and K. Gärtner, *Appl. Surf. Sci.*, 2005, **252**, 1959–1965.

42 I. Milošev, M. Metikoš-Huković and Ž. Petrović, *Mater. Sci. Eng. C*, 2012, **32**, 2604–2616.

43 I. Gouzman, M. Dubey, M. D. Carolus, J. Schwartz and S. L. Bernasek, *Surf. Sci.*, 2006, **600**, 773–781.

44 P. E. . B. K. D. Moulder, J. F. Stickle and W. F. Sobol, *Handbook of X-ray Photoelectron Spectroscopy*, 1993.

45 S. R. Cicco, D. Vona, G. Leone, E. De Giglio, M. A. Bonifacio, S. Cometa, S. Fiore, F. Palumbo, R. Ragni and G. M. Farinola, *Mater. Sci. Eng. C*, 2019, **104**, 109897.

46 L. Rojo, B. Gharibi, R. McLister, B. J. Meenan and S. Deb, *Sci. Rep.*, 2016, **6**, 1–10.

47 M. C. Brochier Salon and M. N. Belgacem, *Phosphorus, Sulfur Silicon Relat. Elem.*, 2011, **186**, 240–254.

48 G. Beamson and D. Briggs, *High resolution XPS of organic polymers, the scienta ESCA300 database*, John Wiley & Sons, Inc, Chichester, ENG, 1992.

49 A. Shimojima, Y. Sugahara and K. Kuroda, *Bull. Chem. Soc. Jpn.*, 1997, **70**, 2847–2853.

50 M. C. Brochier Salon, P. A. Bayle, M. Abdelmouleh, S. Boufi and M. N. Belgacem, *Colloid. Surface. Physicochem. Eng. Aspect.*, 2008, **312**, 83–91.

51 T. Gunji, T. Kasahara and Y. Abe, *J. Sol-Gel Sci. Technol.*, 1999, **13**, 975–979.

52 J. Ren, Z. Li, S. Liu, Y. Xing and K. Xie, *Catal. Letters*, 2008, **124**, 185–194.

53 B. Torun, I. Giner, G. Grundmeier and O. Ozcan, *Surf. Interface Anal.*, 2017, **49**, 71–74.

54 Z. Liu, J. Tabora and R. J. Davis, *J. Catal.*, 1994, **149**, 117–126.

55 J. Landoulsi, M. J. Genet, C. Richard, K. El Kirat, S. Pulvin and P. G. Rouxhet, *J. Colloid Interface Sci.*, 2008, **318**, 278–289.

56 E. Hoque, J. A. DeRose, P. Hoffmann, H. J. Mathieu, B. Bhushan and M. Cichomski, *J. Chem. Phys.*, 2006, **124**, 174710–174716.

57 N. S. McIntyre, H. Y. Nie, A. P. Grosvenor, R. D. Davidson and D. Briggs, *Surf. Interface Anal.*, 2005, **37**, 749–754.

58 S. R. Cicco, D. Vona, G. Leone, E. De Giglio, M. A. Bonifacio, S. Cometa, S. Fiore, F. Palumbo, R. Ragni and G. M. Farinola, *Mater. Sci. Eng. C*, 2019, **104**, 109897.

59 P. M. Dietrich, S. Glamsch, C. Ehlert, A. Lippitz, N. Kulak and W. E. S. Unger, *Appl. Surf. Sci.*, 2016, **363**, 406–411.

60 H. Zarrin, J. Fu, G. Jiang, S. Yoo, J. Lenos, M. Fowler and Z. Chen, *ACS Nano*, 2015, **9**, 2028–2037.

61 R. Tang, Y. Zhang, Y. Zhang and Z. Yu, *Carbohydr. Polym.*, 2016, **139**, 191–196.

62 F. C. Dos Santos, S. V. Harb, M. J. Menu, V. Turq, S. H. Pulcinelli, C. V. Santilli and P. Hammer, *RSC Adv.*, 2015, **5**, 106754–106763.

63 S. D'Elia, V. Barna, N. Scaramuzza, G. Strangi and R. Bartolino, *J. Mater. Res.*, 2009, **24**, 2784–2794.

64 D. Chen, H. K. Y. Wu, S. Naderi-Gohar, Y. Wu, Y. Huang and H. Y. Nie, *J. Mater. Chem. C*, 2014, **2**, 9941–9948.

65 S. Ferraris, M. Cazzola, V. Peretti, B. Stella and S. Spriano, *Front. Bioeng. Biotechnol.*, 2018, **6**, 1–7.

66 F. Borghi, V. Vyas, A. Podestà and P. Milani, *PLoS One*, 2013, **8**, 1–14.

67 K. Suttiponparnit, J. Jiang, M. Sahu, S. Suvachittanont, T. Charinpanitkul and P. Biswas, *Nanoscale Res. Lett.*, 2011, **6**, 1–8.

68 Y. Zhai, X. Zhang, Z. Wu and Z. Wang, *J. Memb. Sci.*, 2020, **597**, 117679.

69 C. Liu, Y. Guo, X. Wei, C. Wang, M. Qu, D. W. Schubert and C. Zhang, *Chem. Eng. J.*, 2020, **384**, 123306.

70 Z. Yang, D. Saeki, R. Takagi and H. Matsuyama, *J. Memb. Sci.*, 2020, **595**, 117529.

71 C. Oueiny, S. Berlioz, L. Patout and F. X. Perrin, *Colloid. Surface. Physicochem. Eng. Aspect.*, 2016, **493**, 41–51.

72 R. Quiñones, S. Garretson, G. Behnke, J. W. Fagan, K. T. Mueller, S. Agarwal and R. K. Gupta, *Thin Solid Films*, 2017, **642**, 195–206.

73 D. Štular, J. Vasiljević, M. Čolović, M. Mihelčič, J. Medved, J. Kovač, I. Jerman, B. Simončič and B. Tomšič, *J. Sol-Gel Sci. Technol.*, 2017, **83**, 19–34.